ICSO 2016

International Conference on Space Optics

Biarritz, France

18–21 October 2016

Sentinel-5: monitoring and correction of charge transfer inefficiency using the instrument spectral response function of the spectrometer

C. Keim

T. Gühne

SENTINEL-5: MONITORING AND CORRECTION OF CHARGE TRANSFER INEFFICIENCY USING THE INSTRUMENT SPECTRAL RESPONSE FUNCTION OF THE SPECTROMETER

C. Keim[1a], and T. Gühne[1b]
[1]*Airbus DS GmbH, 81663 München, Germany.*
[a]*corneli.keim@airbus.com,* [b]*tobias.guehne@airbus.com*

Performance requirements result that todays' imaging spectrometers as Sentinel-5 make use of array CCDs to simultaneously measure the entire spectrum of several adjacent spatial samples. Due to radiation doses accumulated during the mission lifetime, defects acting as traps for charges are generated in the silicon matrix. The charges captured therein result in a drop of charge transfer efficiency i.e. an increase of charge transfer inefficiency (CTI). CTI leads to a faint signal trail for each pixel in the opposite direction to the read out. In spectrographs this results into a smear out of the spectral content, leading to an error in the retrieved trace gas concentrations. However, similar to astronomical and imaging applications, the spectrum can be corrected in the post processing. In this paper an alternative approach is discussed, which incorporates the impact of CTI in the spectral response function (ISRF) of the instrument that consequently allows for monitoring of CTI evolution and correction of its impact.

I. INTRODUCTION

The Sentinel-5 mission [2] focuses on monitoring of trace gas concentrations and aerosols in the atmosphere. The instrument is a high resolution spectrometer system operating in the ultraviolet (270nm) to the short-wave infrared (2385nm) in seven different bands making use of CCD and CMOS detectors.

Charge transfer inefficiency (CTI, [e.g. 3]) has been first observed in silicon CCD's of astronomic instruments based in space. The effect was understood as radiometric error and accordingly corrected for [e.g. 7]. In this paper we discuss how the impact of CTI can be incorporated into the spectral impulse response of the spectrometer, the so called instrument spectral response function (ISRF).

We give an introduction into the physical and mathematical fundamentals of CTI and ISRF and discuss its modelling. The main part is dedicated to the analysis of the expected ISRF evolution due to CTI. Based on measurements of representative breadboard detectors before and after radiation damage, the impact of CTI is assessed. Further we investigate the signal dependence of CTI and show the impact on the ISRF for the theoretical S5 spectra as for real GOME measured data, thus covering the whole scene dynamic.

II. CHARGE TRANSFER IN A CCD DETECTOR

A. *Physical explanation of charge transfer inefficiency*

Charged-coupled devices (CCD) are formed by light sensitive Metal-Insulator-Semiconductor (MIS) diodes fabricated in matrix form [4]. The read out is realized by transferring the charges through the array to the read-out circuit. As there are many pixels in a line, transfer from pixel to pixel must be highly efficient. This transfer is enabled by different processes as diffusion, self-induced drift and the effect of the fringing field. Various clocking schemes allow moving charges among adjacent pixels in a row at rates of several 10 MHz. Thereby the potential depths are varied with the applied gate voltage.

Charge transfer inefficiency (CTI, [1, 5, 6]) is explained by defects, mainly vacancies, generated in the silicon matrix through high energetic particles to which the detector is exposed in orbit. The number of defects increases over lifetime resulting in an even more pronounced CTI. The traps capture photo-electrons generated in the silicon photodiode and release them with a defect specific time constant. When these constants are in the order of the read-out time, the release causes an additional signal and therefore influencing the signal strength in the receiving pixel. Typically CTI results in a tail that is smeared along the read-out direction covering several pixels.

In a CTI versus signal plot, a "tub" like shape is evidence for signal dependence. Different regions can be identified: At the lower and upper end of the signal range relatively strong CTI phenomena are observed, whereas a plateau of lower CTI is present in between.

A simplified picture to describe this dependency can be drawn making use of the band diagram of a MIS diode with a buried channel structure (example for a CCD pixel). The reverse bias voltage applied to the n- and p-doped diode is equal to the surface potential and causes deep depletion (for holes). The bands are strongly bent and the conduction band forms a potential well for electrons, since it is energetically below the Fermi-Level.

When signal (inversion) charges are generated by absorption of photons in the depletion layer, electrons will accumulate in this potential well. Hence at low signal only few electrons are generated in an extended depletion region with a probability of being captured by traps present herein. This results in a relatively large CTI w.r.t. the signal. With increasing signal charge however, the potential well becomes shallower and the depletion region shrinks. The slope of CTI vs. signal decreases and becomes almost flat when a constant CTI is reached, where equilibrium is established when all traps within the channel are filled. High signals in combination with an un-favourable clocking scheme can lead to flushing of the buried channel and hence the electron cloud may extend and reach the surface, where an increased number of surface states will capture carriers and cause again an increase of CTI. This can be prevented by properly orchestrating the CCD operation.

B.   Charge transfer inefficiency modelling

Due to rather early stage of the project Sentinel 5, no radiation affected breadboard detectors are yet available. However, due to similarity to the Sentinel-4 detectors, i.e. same CCD technology and silicon material, first simulations of CTI can be based on results obtained thereof [8].

For S4 as for S5 the charge is transferred in three steps, Image-to-Memory, Memory-to-Register, and Register-to-Output. Each of these transfers introduces CTI effects. The latter, Register-to-Output transfer is along the spatial direction and therefore the serial CTI causes spatial distortion of the spectra. This paper focuses on the spectral performance and therefore the Register-to-Output transfer and the serial CTI effect will be ignored for the remainder of this work. The Image-to-Memory and the Memory-to-Register transfers are along the spectral direction, the parallel CTI therefore causes a spectral distortion of the spectra. As the CTI effects cannot be adapted to the S5 conditions without introducing too many uncertainties, we chose the inverse approach and scaled the S5 expected spectra to the S4 detector. The only parameter taken from S5 is the number of 630 spectral pixels, to allow the simulation of the S5 entire spectral range, considering the split of the image area in two halves, each read out to opposite direction. As all breadboard results are 'per pixel' this modification can be done without introducing an artefact. We use a phenomenological model which excellently reproduces the measurement results. It is based on well-established rate equations that are widely used to model generation and recombination processes in semiconductors. However we did not further detail the origin of each parameter since it is beyond the purpose of the model. The measurement allows for a good fit of a single exponential decay for the parallel CTI. In the model we therefore do not split the parallel transfer in Image-to-Memory and the Memory-to-Register; both are merged in the phenomenological description. Quantitative conclusions are valid in this frame, and will be revised based on future breadboard results dedicated to S5.

Capture and release of electrons in traps is an exponential decay. As the capture time constant is about a factor 1000 shorter than the line transfer period, the simulation can be simplified by removing the time dependency of capture and by only using the limit in the model.

The amount of captured electrons depends on the number of traps and on the signal transferred through the pixel of regard. This dependency can be extracted from the measurements and be expressed as:

$$c = \alpha \cdot \text{Signal}^\beta \tag{1}$$

Where c is the number of captured electrons in this time step, α is a function of the number of traps, and β gives the correct signal dependency. Similarly the expression of the release can be extracted from the measurements to be:
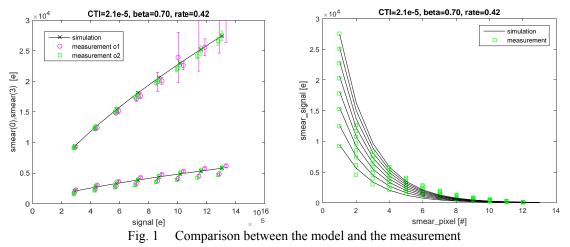
$$r = t \cdot (1 - \exp(-\tau_{lt}/\tau_r)) \tag{2}$$

Where r is the amount of electrons released from the traps into the signal in this time step, t is the number of trapped electrons in the pixel, τ_{lt} is the line transfer period, and τ_r is the release time constant.

For release, the time constant of some trap types is close to the line transfer time, therefore the exponential is kept.

$\alpha = 0.00074997$

$\beta = 0.70$

$(1 - \exp(-\tau_{lt}/\tau_r)) = 0.42$

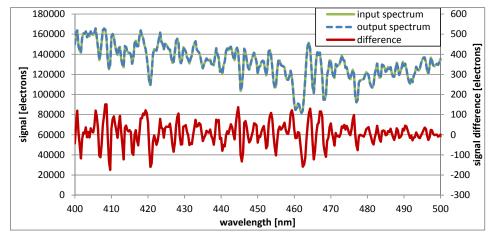Fig. 1 compares the the S4 measurements with the simulation, and shows the good capability of the model to correctly describe CTI in the CCD.

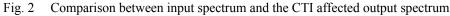Fig. 1   Comparison between the model and the measurement

C.   Charge transfer inefficiency and its impact on a spectrum

Comparing the incident spectrum onto the detector with the read-out spectrum, now altered by parallel CTI, it becomes evident, that the signal of each pixel is altered (see Fig. 2). Obviously, CTI can be understood as a radiometric error.

Further, comparing spectral regions containing shallow absorption lines with regions where deep absorption lines are present (see Fig. 2 and Fig. 3), it is seen that the impact of CTI is largely depending on the spectral structure. In particular, a constant signal is almost unaffected by CTI. Attempts to fit the line-shape of the instrument spectral response function to the CTI altered read-out spectrum, results in broadened and shifted spectral lines. Hence, the effect of CTI can be alternatively understood as a spectral impact. In this paper we focus on the latter interpretation of CTI and show that it allows to fully describing the radiometric error as well.

A direct consequence of a spectral interpretation is that there is no radiometric correction of the CTI affected spectra necessary in the L1b process. But the spectral properties of the spectrum will be adapted in the L1b process.
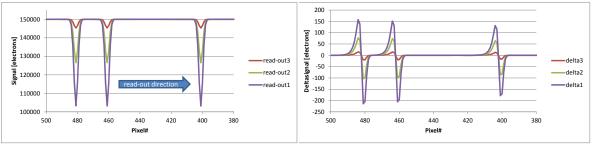

Fig. 2   Comparison between input spectrum and the CTI affected output spectrum

Fig. 3   Illustration of the CTI as spectral effect

D. Matrix representation of Charge transfer

We can simulate the effect of CTI on a measured spectrum by applying the CTI model to any test spectrum. As test spectrum a top of atmosphere (TOA) spectrum is used, convolved with a Gaussian ISRF, and scaled to fit to the detectors full well. This approach separates the CTI impact from any other radiometric or spectral error source,

$$L_{CT,1} = CTI\_model\ (L_{opt}) \tag{3}$$

where L_{opt} is the scaled TOA spectrum convolved with the optical ISRF. $L_{CT,1}$ is the spectrum read out from the detector, which is affected by CTI.

It can be shown that the effect of CTI on a spectrum can be expressed as a matrix-multiplication:

$$L_{CT,2} = M \cdot L_{opt} \tag{4}$$

Here M is a NxN matrix, fulfilling the condition $L_{CT,1} \approx L_{CT,2}$. M can be derived from the CTI model by running the model on "unity vectors", i.e. test spectra which are zero except for exactly one spectral value which corresponds to the TOA test spectrum:

$$M(i,:) = CTI\_function(\ u_i \cdot L_{opt}(\lambda_i)\ ) \tag{5}$$

where u_i the i-th unit-vector $(0,0,...0,1,0, ... 0)$, with "1" at position "i", M(i,:) the lines of M, and $L_{opt}(\lambda_i)$ the intensity of the i-th spectral position.

Fig. 4 compares the two CTI affected spectra ($L_{CT,1}$ and $L_{CT,2}$) for an example. The spectrum incident on the detector is the VIS reference spectrum for S5 taken from the radiometric model. The UV2VIS detector of S5 is a split-frame detector, where the two halve spectra are read out to the opposite edges. For the simulation, the split wavelength was set to exactly 400nm. In the figure we show the upper half where the read-out direction is to the right, causing the largest errors due to CTI in the left part of the spectrum.
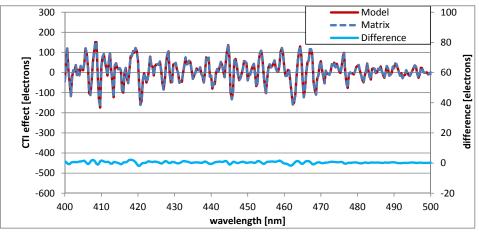

Fig. 4   The figure shows on the left axis the radiometric difference between incident spectrum and read-out spectrum for the two cases: i) the read-out spectrum is simulated with the CTI model (red solid), see (3) and ii) the read-out spectrum is calculated as matrix multiplication (blue dashed), see (4). The difference is so small that the 'matrix' curve hides the 'model' curve; the difference is given also in light blue on the right axis.

III. ISRF

The ISRF is the spectral response of one instrument to a monochromatic stimulus. Its practical use in the Level-2 is to derive the spectrum measured by an instrument from the monochromatic spectrum entering the instrument. The monochromatic spectrum e.g. results from a radiative transfer model.

Accordingly, the ISRF is defined in the System Requirements Documents of S5 as:

$$L'(\lambda_0) = \int_0^\infty ISRF(\lambda, \lambda_o)L(\lambda)d\lambda \tag{6}$$

For practical reasons (i.e. a) the ISRF and the spectrum L are available on a sampled grid, and b) the computation of an integral is done as a sum) the integral is usually replaced by a sum:

$$L'(\lambda_0) = \sum_i ISRF(\lambda_i, \lambda_0) \cdot L(\lambda_i) \cdot \Delta\lambda \tag{7}$$

A.   Mathematical representation of the ISRF as matrix

In the sum in (7), the spectra L' and L are one-dimensional functions, sampled on one-dimensional grids. This is nothing else then vectors. Similarly the ISRF is a two-dimensional function, sampled on a two-dimensional grid. This is a matrix. The above sum can then be written more compact

$$L'=ISRF*L \tag{8}$$

The convolved spectrum L' is sampled on the N detector pixels, being a 1xN vector. The monochromatic TOA spectrum L has a much finer sampling, say K samples. L is a 1xK vector. The Matrix ISRF is thus NxK to fit into the equation.

Note that the ISRF in all equations is normalised to ensure that the measured energy equals the incident energy. The term $\Delta\lambda$ in (7) is subject to the normalisation and therefore included in the ISRF matrix in (8).

To aid the reader, the matrix and the vectors in (8) are expanded below:

$$\begin{pmatrix} L'_1 \\ L'_2 \\ \vdots \end{pmatrix} = \begin{pmatrix} measured\ spectrum\ in\ pixel\ 1 \\ measured\ spectrum\ in\ pixel\ 2 \\ \vdots \end{pmatrix} = \begin{pmatrix} ISRF_{pixel1}(\lambda_i) \\ ISRF_{pixel2}(\lambda_i) \\ \vdots \end{pmatrix} * \begin{pmatrix} L(\lambda_1) \\ L(\lambda_2) \\ L(\lambda_3) \\ L(\lambda_4) \\ \vdots \end{pmatrix} \tag{9}$$

The i-th entry/line of (8) reads $L'(\lambda_i) = ISRF(\lambda_i, \lambda_j) * L(\lambda_j)$, which is (7).

Combining (4) with (8) leads to a fundamental approach of understanding: It is equivalent to apply CTI on the spectrum or to apply CTI only on the ISRF.

$$L_{\text{CTI}} = M * [ISRF * L] \tag{10}$$

$$L_{\text{CTI}} = [M * ISRF] * L \tag{11}$$

B.   ISRF change by charge transfer inefficiency

As shown above (III.A), the impact of CTI onto a spectrum can be understood as the impact of CTI onto the ISRF. This leads to naively unexpected changes of the ISRF, e.g. with the pixel number in the CCD, which are detailed below.

As the trapping/release process is dominated by the number of traps, it is clear that the relative impact on the signal is larger for low signals and smaller for huge signals (see Fig. 5). From the measurements, the signal dependency of capture can be described with a power-law (see (1)). As only captured electrons can be released, the release shows the same, indirect, dependency on the signal.

The charge of a given pixel in a CCD is read out through all pixels between the pixel of regard and the register. At each transition from one to the next pixel the transported charge is altered, some charge is lost by trapping in the old pixel and some charge is added by release in the new pixel. As long as only a small amount of the transported charge is affected by trapping/release the shape of the signal remains similar and each of the transitions is very equal. The more transitions a signal sees, the more it is affected. Fig. 6 shows the dependency of broadening (left panel) and shift (right panel) on the position of the incident test signal on the detector. The test signal is a Gaussian which represents the pure optical ISRF. The test signal is equal for all positions, and always centred to the pixel. Fitting a Gaussian to the CTI affected readout signal shows that the Gaussian is broaden and shifted wrt the incident test signal. Fig. 6 shows both, the relative broadening and the shift, and the signal dependency explained in the preceding paragraph.

The number of traps increases over lifetime due to radiation. Assuming a linear increase of the number of traps over time, the impact of CTI on the ISRF is also linear over time. All figures in this work have been calculated for the maximum CTI effect at end-of-life of the instrument.
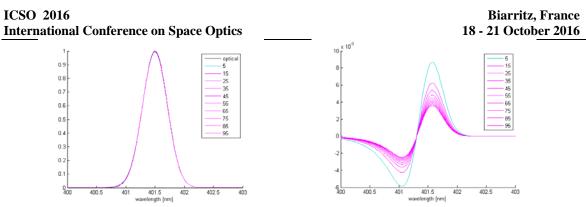
Fig. 5   The figure shows the optical ISRF together with the CTI distorted ones, for several signal levels (5% .. 95% of CHC) in the left panel. The right panel give the differences between the optical ISRF and the CTI distorted ones. The figures are for pixel 10, just after the split, where the effect is largest within the spectral range (worst case).
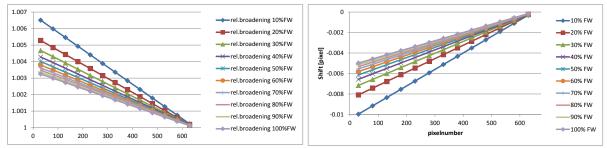

Fig. 6   The figure shows the broadening and shift of the read-out spectral line shape compared to the incident optical one.

C.   Approach for Sentinel-5

In the case of Sentinel-5, both, the radiometric accuracy and the ISRF knowledge accuracy are controlled by requirements. We decided to understand and treat the CTI impact on the spectra as spectral effect, i.e. the impact of CTI is fully described by its effect on the ISRF. Therefore CTI only needs to be accounted for in the breakdown of the two requirements controlling the knowledge accuracy of the ISRF, which are cited below:

INS-410   *The ISRF shape shall be known to an accuracy better than 2.0% of the peak value of the ISRF in the spectral range Λ where the ISRF is at least 2% of the peak value.*

INS-430   *The FWHM of the ISRF shall be known to an accuracy of 1%.*

The optical component of the ISRF varies over the spectral range and with the field angle; therefore it is clear that the dependency of the strength of the CTI impact on the pixel position can be easily incorporated into the existing spectral variation.

Formally the signal dependency and the time dependency of the CTI can be accounted for by delivery of an ISRF set for each measured spectrum. As this is not very convenient, it is intended to have a small number of ISRF sets, covering the signal dynamics, which are valid for a time period and which are updated from time to time. In the frame of this paper we use an allocation of 0.4% for CTI related ISRF shape knowledge accuracy.

1.   EOL assessment with the (theoretical) reference spectra

In the frame of Sentinel-5, four representative spectra for Earth reflected radiance have been provided. They are derived for spectrally constant albedo (i.e. min=5% and max=100%) and the absorption of a standard atmosphere. The different angles through the atmosphere over the orbit have been accounted for by proving high latitude spectra with solar zenith angle of SZA=75° and tropical spectra with SZA=0°. From these reference spectra, spectra for any albedo can be interpolated for both latitude regions.

For each spectral sample the CTI-affected ISRFs have been simulated for any albedo and both latitude regions. For each latitude region and each spectral sample, one median ISRF (see Fig. 7) has been generated from those simulations, which are showing the smallest difference to the total of ISRFs of all albedos.

For the tropical latitude region, Fig. 8 shows for all spectral samples (300-500nm) and all albedos (5-100%) the maximum absolute difference of the ISRF to the median ISRF. Note the plotted pseudo-spectrum is constructed by the individual differences per spectral sample. By construction the median ISRF has the same difference to the two extreme ISRFs (i.e. albedo 5% and 100%) and therefore plotted onto each other. The resulting shape

error is up to 0.2% for the various albedos, leaving sufficient allocation to account for further degradation of the transfer efficiency. Extending the calculation of the median ISRF to the high latitude region, also results into a shape error of up to 0.2% (see Fig. 9).
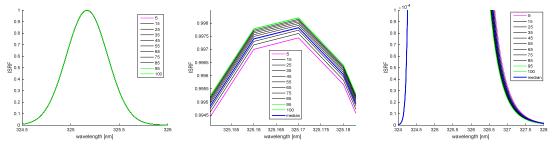

Fig. 7   The CTI affected ISRF for several albedo values together with the median ISRF in all panels. The middle and right panels show zooms to highlight the important affects.
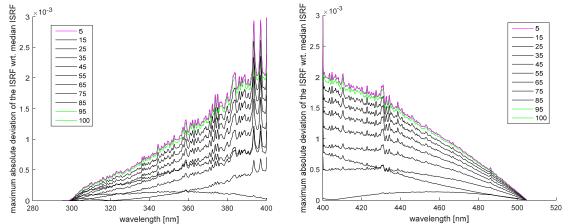

Fig. 8   The figure shows the maximum absolute deviation of the CTI distorted ISRF from the median ISRF. The two panels show the two detector halves. Both panels give the curves for a set of albedo levels going from 5% to 100%.
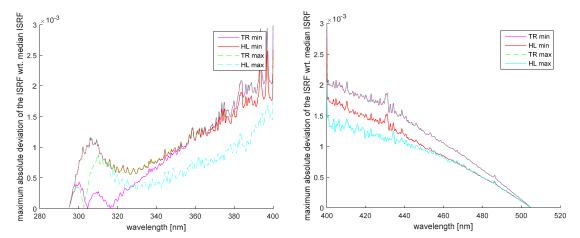

Fig. 9   The figure shows the maximum absolute deviation of the CTI distorted ISRF from the median one. The two detector halves are shown in the left, respectively right panel. Both panels give the curves for the maximum and the minimum radiance in the two latitude regions, tropical (TR) and high latitude (HL).

2.   *EOL assessment with one orbit of GOME measured spectra*

As the theoretical spectra, limiting the S5 dynamic range may not reflect the real situation; the simulation was fed with one orbit of GOME measurements. Looking at the spectra, it is obvious that the upper limit in the dynamic range (100% albedo) is never reached by real spectra. The maximum GOME radiance equals an albedo

of 65%. The GOME data set also shows negative radiances, likely unphysical, which are discarded from the analysis. In the ISRF assessment the GOME dataset was split in two subsets, the first covering spectra within the S5 dynamic range, and the second containing spectra of radiances below the S5 specified minimum. Remember, the median ISRF was derived for the S5 dynamic range, so we expect larger errors for spectra of lower radiances. In order to get rid of the uncertainty of the real ISRF of the GOME instrument, and also of its spatial and spectral variation, the GOME measurement was used as monochromatic input to S5 and further processed with the same artificial Gaussian ISRF as used before. The deviation of the CTI affected ISRF from the S5 median ISRF is shown in Fig. 10 for both GOME subsets over the entire orbit. For radiances below the S5 minimum spectra (magenta curves), the CTI distorted ISRF deviates by 0.8% from the S5 median ISRF, for the spectra within the S5 dynamic range (black curves) the deviation is below 0.2%, well within the allocation.
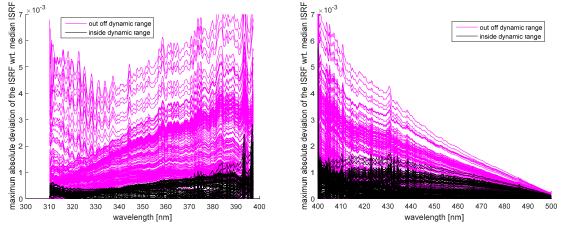

Fig. 10   The deviation of the CTI affected ISRF of GOME measurements from the S5 median one. GOME spectra with radiances lower than the S5-minimum radiance are plotted in magenta.

IV. CONCLUSION

We have shown an alternative approach to deal with the impact of charge transfer inefficiency on a measured spectrum. Instead of correcting the radiometric impact, we understand the effect as spectral and derive a median CTI affected ISRF which is provided together with the measured L1b spectra for the use in the Level2 process. The deviation of the real and median ISRF is below 0.2%, independently shown on two different sets of TOA data, the S5 reference spectra and GOME-2 results. This value is well within the required limit. It is interesting to note that even for GOME scenes which are well below the S5 minimum, the CTI affected ISRF shape error is as low as 0.8% and therefore may still fit in a reasonable allocation of the total tolerable ISRF shape error.

V.   REFERENCES

[1] Banghart, E. K.; Lavine, J. P.; Trabka, E. A.; Nelson, E. T.; Burkey, B. C., "A model for charge transfer in buried-channel charge-coupled devices at low temperature", IEEE Transactions on Electron Devices, vol. 38, issue 5, pp. 1162-1174

[2] Bartsch, P., Gühne, T., Seefelder, W., Status of design, performance and development, Proceedings of the International Conference on SpaceOptics (ICSO), Biarritz, France, 18-21 Oct. 2016, in print.

[3] Grant, C.E., Bautz, M.W., Kissel, S.E., & LaMarr, B. 2004, "A charge transfer inefficiency correction model for the Chandra Advanced CCD Imaging Spectrometer", in High-Energy Detectors in Astronomy, Proc. SPIE, 5501, 177 (astro-ph/0407199)

[4] Grundmann, M., "The Physics of Semiconductors, An Introduction including Nanophysics and Applications, 3rd edition2", Springer, Heidelberg, 2016, ISBN 978-3-319-23879-1

[5] Hardy, T.; Murowinski, R.; Deen, M. J., "Charge transfer efficiency in proton damaged CCD's", IEEE Transactions on Nuclear Science, vol. 45, issue 2, pp. 154-163

[6] Hopkins, I. H.; Hopkinson, G. R.; Johlander, B., "Proton-induced charge transfer degradation in CCDs for near-room temperature applications", IEEE Transactions on Nuclear Science, vol. 41, issue 6, pp. 1984-1991

[7] Irizar, J., Gulde, S., Skegg, M., Levillain, Y., Weber, H., Radiation induced charge transfer inefficiencies (CTI) in the Sentinel-4 instrument: modelling, characterization, and correction, Proceedings of the International Conference on SpaceOptics (ICSO), Biarritz, France, 18-21 Oct. 2016, in print.

[8] Levillain, Y., et al., CCD charge transfer inefficiency impact on spectrometer case of Sentinel-4, Proceedings of the International Conference on SpaceOptics (ICSO), Biarritz, France, 18-21 Oct. 2016, in print.